Single fluxon dynamics in Nb-based Josephson junction stacks

J. Zitzmann and A. V. Ustinov
Physikalisches Institut III, Universität Erlangen, D-91058 Erlangen, Germany

M. Levitchev
Institute of Thin Film and Ion Technology, Forschungszentrum Jülich, D-52425 Jülich, Germany

S. Sakai
Electrotechnical Laboratory, 1-1-4 Umezono, Tsukuba-shi, Ibaraki 305, Japan
(September 5, 2000)

Single fluxon dynamics in 5-, and 10-fold vertically stacked Nb-Al/AlO_x-Nb Josephson tunnel junctions is investigated experimentally in dependence of temperature. Numerical simulations are used to gain insight in the dynamics of the system. Detailed account is given on the role of linear oscillations in Josephson multilayers. The locking of the fluxon to the emitted Cherenkov waves is observed at low temperatures. At high temperatures non-ballistic behavior of the vortex is reported and explained by radiation losses. Experimental data, simulation and analytical model are in good agreement and show a clear picture of the dynamics of the phase difference in the multilayer.

I. INTRODUCTION

Reinhold Kleiner's and Paul Müller's finding of the intrinsic Josephson effect in highly anisotropic high-T_c superconductors[1] gave a great impetus to the research in the field of Josephson physics. Anisotropic high-T_c superconductors are in essence vertical stacks of Josephson junctions produced by nature. Due to the close spacing of the superconductor-insulator lattice, the superconducting screening currents range across Many layers and induce a coupling between the individual junctions. The dynamics of magnetic flux quanta in such systems has raised a lot of interest. These Josephson junction multilayers are good candidates for high power flux-flow oscillators as shown in simulations[2,3]. Yet the predicted in-phase mode is still to be confirmed experimentally.

To investigate the mechanisms that govern the fluxon dynamics in high-T_c multilayers we mimic them by stacking artificially made $\mathrm{Nb-Al/AlO_x-Nb}$ junctions[4]. This approach allows to control the properties of the samples in a wide range. In particular, the coupling of the junctions can be adjusted easily by varying the thicknesses of the Nb-films. Therefore these multilayers can be tailored for experimental and application purposes. At present artificial stacks with as many as 28 junctions have been produced, whith a typical spread of the critical currents below 10%. This makes the low-T_c systems an ideal counterpart to high-$\mathrm{T_c}$ mesa structures, where the number of achievable junctions ranges between a few and several hundreds.

Regarding possible applications, the fluxon dynamics is a most interesting field to investigate in multilayers. While the properties of artificial twofold stacks are by now thoroughly explored[5–9], Josephson systems with a larger number of junctions N were not yet experimentally investigated. Yet, before moving on to the flux-flow regime, it has proven to be inevitable to learn about the particular dynamic states in multilayers, as their behavior differs greatly from the one found in single junction flux-flow oscillators. Here, it was our primary objective to find the mechanisms involved in the motion of fluxon in stack by investigating single vortices in $(\mathrm{Nb-Al/AlO_x})_N - \mathrm{Nb}$ systems. To interpret the experimental data, we thoroughly compare them with the results of numerical simulation.

The paper is organized as follows. In section II we review the SBP model which describes the dynamics of the phase differences in stacks and also discuss linear modes. The experimental results are presented and compared with the simulations in section III. Specific dynamic regimes at various temperatures are discussed in detail. Section IV concludes the work.

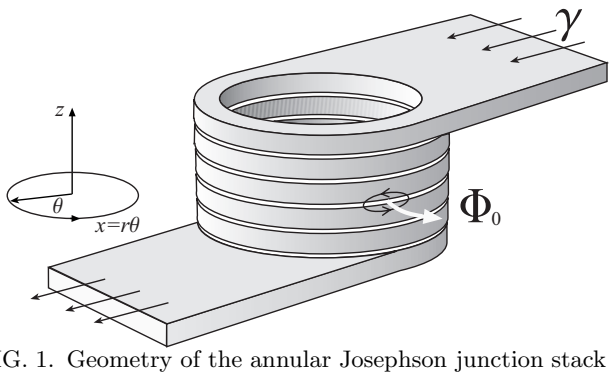

FIG. 1. Geometry of the annular Josephson junction stack of $N = 5$ junctions; a fluxon is accelerated clockwise under the influence of the (normalized) bias current $\gamma = I/J$.

II. THEORETICAL MODEL

An N-fold stack of long Josephson junctions, consisting of N insulating and $N+1$ superconducting layers (see Fig. 1), is well described by the Sakai-Bodin-Pedersen model of inductively coupled sine-Gordon equations[10]. The N equations which govern the phase dynamics in the Josephson stack can be written as

$$\frac{\hbar}{2e\mu_0}\partial_{xx}\phi_l = s_{l-1}\, j^z_{l-1} + d'_l\, j^z_l + s_l\, j^z_{l+1}\,, \qquad (2.1)$$

where $l = 1 \ldots N$, and

$$j^z_l = \frac{\hbar}{2e} C_l\, \partial_{tt}\phi_l + \frac{\hbar}{2e} G_l\, \partial_t \phi_l + J_l\, \sin\phi_l - I_l$$

is the total current flowing through junction l in z-direction. Here C_l, G_l, J_l, and I_l denote the unit area capacitance, conductance, critical current and bias current respectively. Furtheron we assume that the junctions are connected in series and,therefore, receive the same bias current $I_l = I$ for all l. Also the parameters $G_l = G$ and $C_l = C$ are taken equal for all layers. The effective junction thickness d'_l and the coupling parameter s_l are defined in Ref. 10. The fact that the limit of $s \to 0$ of Eq. (2.1) yields the set of N uncoupled sine-Gordon equations makes clear that the coupling is induced by the currents flowing in the adjacent superconducting layers.

Neglecting the quasiparticle damping and inserting an ansatz of linear traveling waves $\phi_l = A_l \exp(i(kx - \omega t))$ with small amplitude into Eq. (2.1) yields the dispersion relation

$$\omega_m^2 = \omega_p^2 + \left(c_m^{(N)}\right)^2 k^2 \quad \text{with} \quad m = 1, \ldots, N\,, \qquad (2.2)$$

where $c_m^{(N)}$ are called characteristic velocities. For a stack with equal junction these velocities can be calculated according to $c_m^{(N)} = \bar{c}\left[1 + 2\frac{s}{d'}\cos\left(\frac{m\pi}{N+1}\right)\right]^{-1/2}$, where $\bar{c}$ is the Swihart velocity calculated from the single junction parameters. In the case of non-homogeneous stack the characteristic velocities can be caculated by solving the eigenvalue problem of the coupling matrix from (2.1)[4]. Note that, unlike in single long junctions, the maximum velocity of fluxons in stacks is generally unknown[7] and does not necessarily coincide with the minimum phase velocity of linear waves $c_N^{(N)}$. In particular fluxon motion at velocities faster than $c_N^{(N)}$ is possible, which leads to excitation of Cherenkov-like traveling waves by the fluxon[5].

Since an analytical treatment of Eq. (2.1) is hardly possible, numerical simulations prove to be the most valuable tool for gaining insight in the phase dynamics of Josephson junction stacks. The numerical procedure that we employ for solving Eq. (2.1) is based on the finite difference scheme described in Ref. 11. To check the accuracy of the algorithm, we have compared our results with those of simulation routine by R. Kleiner et al.[2], which applies a Fourier expansion method to solve Eq. 2.1. Good agreement between the results of both algorithms has been found[12].

III. RESULTS

Single fluxon states were prepared and measured in samples of $N = 5$ and $N = 10$ junctions with a length L of 418 μm and 597 μm (cf. table 1). The thicknesses of the superconducting Nb films is comparable to the London penetration depth λ_L of 90nm at 0K, so that strong coupling is achieved. We used a ring-shaped (annular) geometry of the stack (see Fig.1) in order to exclude the influence of the junction edges and study of the fluxon motion under periodic boundary conditions.

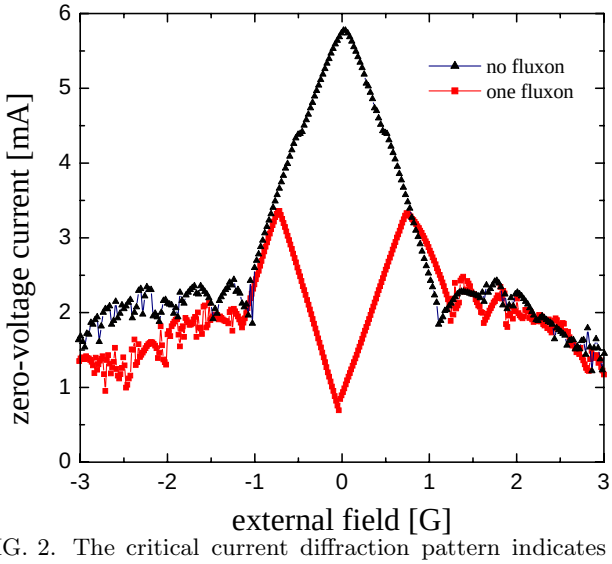

FIG. 2. The critical current diffraction pattern indicates the number of trapped fluxons (shown for sample #2).

To induce a vortex into the system, the samples are cooled through the critical temperature $T_c = 9.2$ K while a small bias current was applied. Below T_c the number of vortices trapped in the junctions is conserved due to the magnetic flux quantization and the topology of the sample. Since trapping of vortices in Josephson multilayers turned to be considerably more difficult than in single junctions, great care was taken to determine the resulting state. With a measurement of the current-voltage characteristic (CVC) the number of unpinned vortices in the stack was determined from the maximum voltage of the fluxon step. Furthermore, the critical current diffraction pattern was measured (see Fig.2) to check the obtained state[13,5]. This method is also a sensitive probe for the pinning of the vortex by defects or parasitic flux in the films.

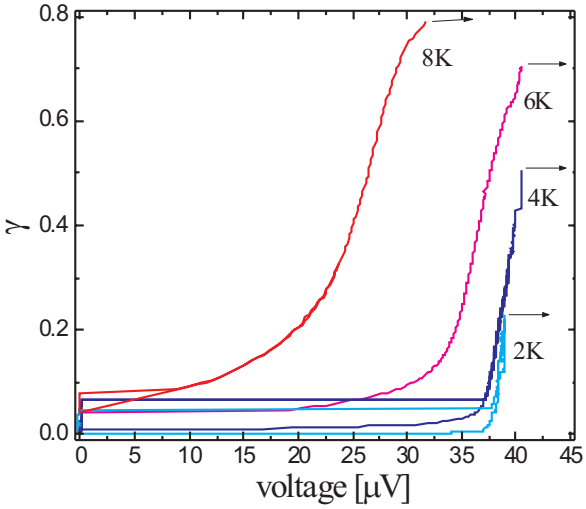

FIG. 3. Measured CVCs of a single fluxon in the center barrier of sample #3; the labels on the curves indicate the temperature.

The measurements were conducted at several temperatures ranging between 1.3 K and 9.2 K. Since the quasiparticle tunneling G depends exponentially on temperature, the damping in the system is controlled by varying the temperature. A typical set of measurements is shown in Fig.3. Note that at low temperatures resonances appear on the fluxon step, which vanish as the temperature is increased. Yet close to T_c, the fluxon step does not approach any asymptotic velocity as found in single long junctions, but shows an S-shape. In the following sections the fluxon dynamics in the low and high temperature regimes is analyzed with the help of numerical simulations of Eq. (2.1).

A. Low damping regime

At low temperature the damping due to the quasiparticle conductance G is sufficiently low so that traveling waves have significant influence on the dynamics of the fluxons. The condition under which Cherenkov waves can be excited is the equality of the fluxon velocity v_{fluxon} with the phase velocity of linear waves $v_{\text{phase}} = \frac{\omega}{k}$. In the limit of no damping, the periodic boundary conditions in the samples imply that only waves with discrete wave numbers $k_h = \frac{2\pi}{L}h$ can be exited, where $h = 1, 2, \ldots, \infty$ is the number of the mode.

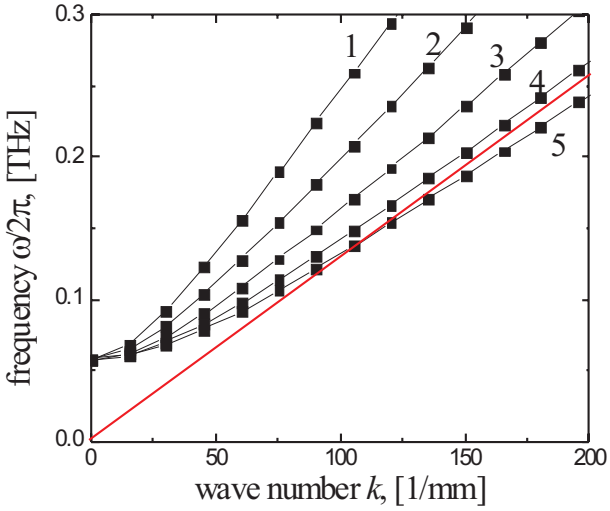

FIG. 4. Plasma dispersion relation for a fivefold stack equivalent to sample #3: the numbers indicate the dispersion branch m, squares the resonant modes h and the straight line the fluxon velocity v_{fluxon}

Using the dispersion relation for linear waves (2.2), one finds that Cherenkov modes are excited at a fluxon velocity of

$$v_{\text{res}} = \sqrt{\left(c_m^{(N)}\right)^2 + \left(\frac{\omega_p L}{2\pi h}\right)^2}\,. \tag{3.1}$$

From this it is clear that the lowest characteristic velocity $c_N^{(N)}$ plays the role of a lower bound to the fluxon velocities at which Cherenkov radiation exists. The excitable modes are plotted in Fig. 4 for sample #3.

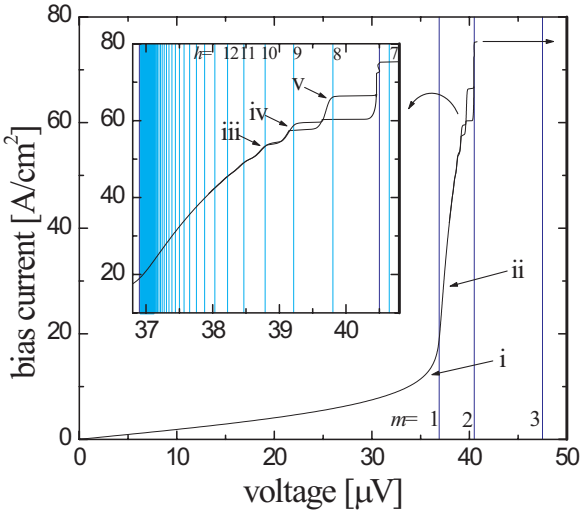

FIG. 5. Simulated CVC of a single fluxon in the center barrier of sample #3 at 4.2K: vertical lines in the main plot indicate the characteristic velocities $c_m^{(N)}$, the lines in the inset show the voltages corresponding to the resonant velocities v_{res} of the mode h.

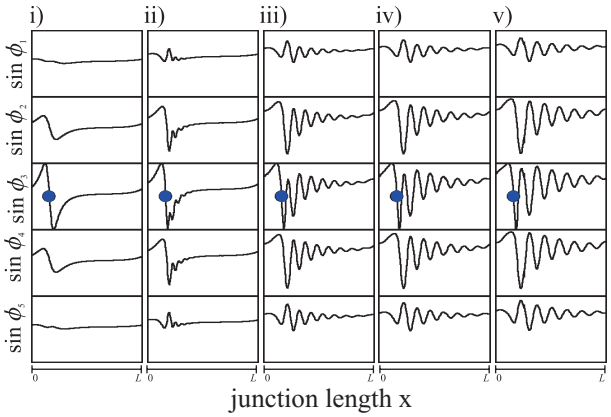

FIG. 6. The simulated profiles of $\sin\phi_l$ in sample #3 with a fluxon in the center barrier for the bias points indicated in Fig. 5: $\gamma_{(\mathrm{i})}$=0.07, $\gamma_{(\mathrm{ii})}$=0.22, $\gamma_{(\mathrm{iii})}$=0.38, $\gamma_{(\mathrm{iv})}$=0.42, $\gamma_{(\mathrm{v})}$=0.47; the fluxon is marked by a circle.

To test whether this prediction is correct, the phase dynamics of a single fluxon in the center junction of sample #3 is simulated using the junction parameters at 4.2 K, specifically J=140 A/cm^2 and C=3.2 μF/cm^2. Although the tunnel conductance can be deduced from the non-relativistic part of the CVC, for numerical analysis a conductance of G=60 kS/cm^2 is used. This is about twice the real value of G at 4.2 K to reduce the computation time. All other parameters for the simulation were either known from the sample fabrication (e.g. the dimensions) or could be obtained by simple measurements (e.g. the critical current). Because of the extremly long calculation times at low damping, we also refrained from a detailed numerical analysis of data obtained at temperatures lower than 4.2K. Fig. 5 shows the CVC of a fluxon captured in the center junction of the sample #3 at 4.2 K, while the profiles of the sine of the phase differences at the bias points labelled in roman are plotted in Fig. 6. The vertical lines with arabic labels in the inset of Fig. 5 correspond to the analytically calculated resonant velocities v_{res} and demonstrate excellent agreement of the expected resonance positions with the simulated data.

With the aid of the simulated phase differences it is now possible to understand the dynamics of the fluxon in the stack: At fluxon velocities lower than the lowest characteristic velocity $c_5^{(5)}$ in Fig. 6i, one can identify the fluxon in the center barrier and its images in the other junctions. When v_{fluxon} exceeds $c_5^{(5)}$, an oscillating tail of Cherenkov radiation arises. Fig. 6ii shows that the amplitude of these waves quickly decays in space and time due to the non-zero damping. With increasing velocity the fluxon excites lower modes h and the wavelength of the radiation increases. In addition, the amplitude of the Cherenkov wake and therefore its length grow. Once the Cherenkov wake extends over the circumference of the junction, the fluxon will interact with the tail it excited and v_{fluxon} locks to v_{res}. Intuitively it is clear that the fluxon is trapped in the potential created by its wave-tail and can overcome v_{res} only if the driving force γ exceeds the force due to this potential. Therefore v_{fluxon} is discretized and hysteretic resonant steps appear on the CVC. These in turn can be assigned to the different modes h of the Cherenkov radiation as illustrated in Fig. 5.

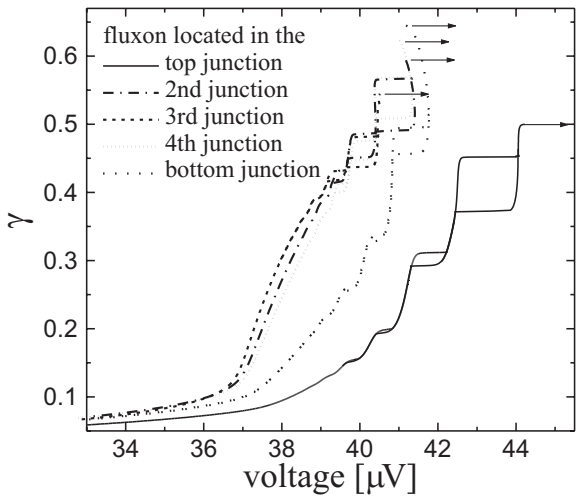

FIG. 7. High velocity range of simulated CVCs of all possible single fluxon states in sample #3: The different curves correspond to fluxons being located in different junctions.

To compare the experimental data with the simulation we present data from sample #3 measured at 4.2 K. Other samples show quite similar results. For single fluxon states measured in experiment it is not known a prioriin which out of N junctions the fluxon is trapped. Nevertheless, the comparison of the measured data with the simulations enables us to determine the junction in which the vortex is located. This can be decided from the features of the relativistic part of the CVC, such as its shape and curvature, as well as the positions of the resonances and their switching current. The simulated CVCs for all possible single fluxon states are presented in Fig. 7. Physically, the distinction is possible for the top and bottom junctions, because they are lacking a neighboring junctions in one of the directions. The distinction between the bottom and top junction themselves can be made due to the difference in thickness of the top and bottom Nb film (see table 1). Still, fluxon states with vortices in the inner junctions cannot be determined with such good confidence.

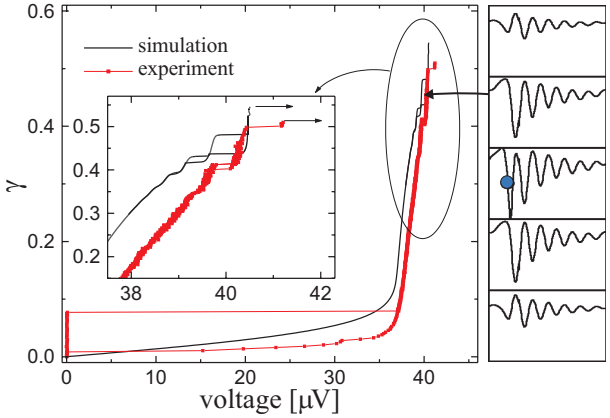

FIG. 8. Measured and simulated CVC of a single fluxon in the center junction of sample #3; the onset shows the profile of the phase differences at the marked point.

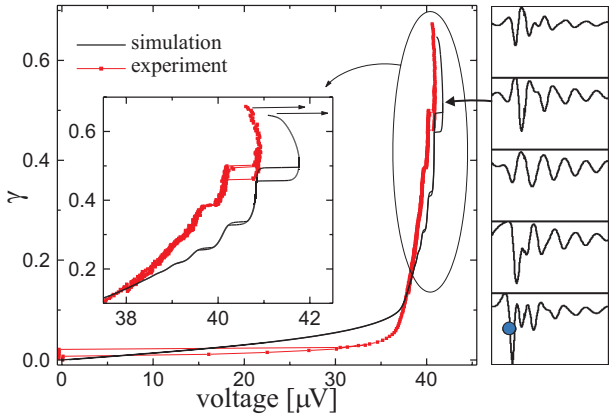

FIG. 9. Measured and simulated CVC of a single fluxon in the bottom junction of sample #3; the onset shows the profile of the phase differences at the marked point, note the negative differential resistance on the top of the fluxon step.

The experimental data in Fig. 8 and Fig. 9 show two different single fluxon states in the 5-fold stack #3. The differences in the measured CVCs enable us to conclude that the fluxon is located in one of the center junctions (Fig. 8) or in the bottom junction (Fig. 9). Cycling through T_c several times allows to catch various fluxon states. It was possible to reproduce identical CVCs and therefore identical fluxon states, which reflects the high quality of the samples. The disagreement in details between the simulated and measured CVCs is mainly due to the discrepancy in G, as simulations using slightly varied parameters show.

B. The crossover between the low and high damping regime

As mentioned above, an increase in temperature drastically raises the quasiparticle tunneling and, therefore, the damping in the stack. Yet because of its topological solitonic nature, the fluxon remains stable. Excited oscillations on the contrary are damped by the increased conductance G. In consequence, the length of the wave-tail created by the vortex will decrease and the resonances on the fluxon step will cease to exist (cf. Fig. 3).

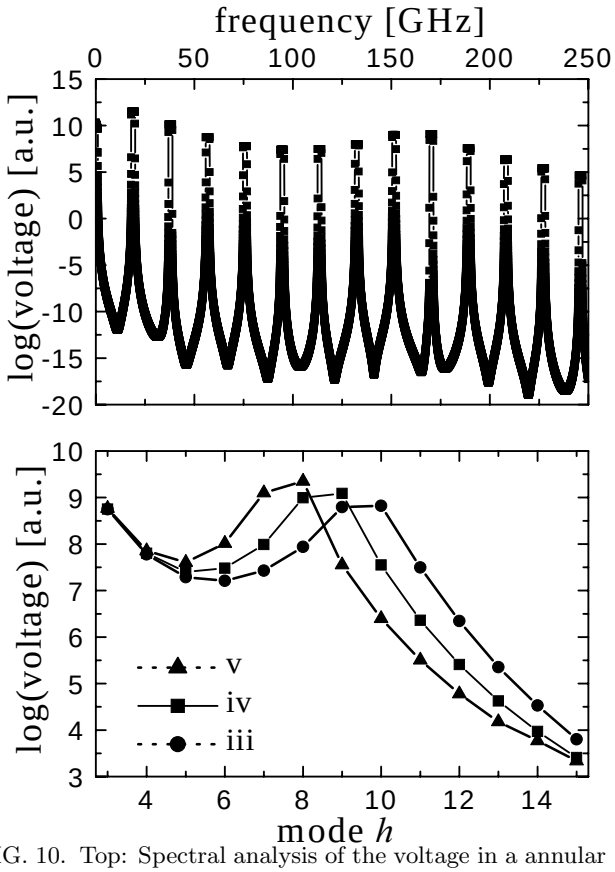

FIG. 10. Top: Spectral analysis of the voltage in a annular fivefold stack at resonance (iv) in Fig. 5. Bottom: Excitation of the modes h at the resonances (iii), (iv) and (v) from Fig. 5

Another general effect associated with the damping of linear modes is the broadening of the linewidth. Specifically, in the Josephson stack, quickly decaying wave-tails do not strongly lock to the periodicity of the sample anymore so that a broader spectrum of waves can be excited. To gain insight into the nature of the broadening of the linear modes, a spectral analysis of the voltages in the stack was calculated by simulation. The parameters for the simulations were again chosen to agree with the characteristics of sample #3 at 4.2K. To determine the Cherenkov mode h that is excited at the resonances (iii) to (v) in Fig. 5, a Fourier transform of the voltage across the stack at an arbitrary spatial point is evaluated. The spectrum of the sampled data at $\gamma_{(\mathrm{iv})}$=0.42 in the top plot of Fig. 10 corresponds to a periodic set of harmonics. Considering that the voltage in the time domain will always peak when the fluxon and it's images move by the sampling point, this is to be expected: The fundamental frequency — the Josephson frequency — here of 18.9 GHz is associated with the fluxon velocity and its

higher harmonics occur at integer multiples of this frequency. The high power of the harmonics is due to the sharpness of the voltage peak in the time domain, which is caused by the fluxon passing the sampling point.

We find a rise in the amplitude of the harmonics ranging from approximately 130 GHz to 200 GHz. Knowing that the fluxon velocity locks to v_{res}, the radiation emitted from mode h adds to the hth fluxon harmonic. To determine which modes are excited at the resonances indicated by (iii), (iv) and (v) in in Fig. 5, the local maxima of the Fourier spectrum are shown in the bottom plot of Fig. 10. Clearly not only a single Cherenkov mode is excited at a time, i.e. the modes broaden significantly already at quite low damping. Also note that the exited mode numbers h=8, 9, 10 from the simulation nicely coincide with the analytical prediction plotted in Fig. 5.

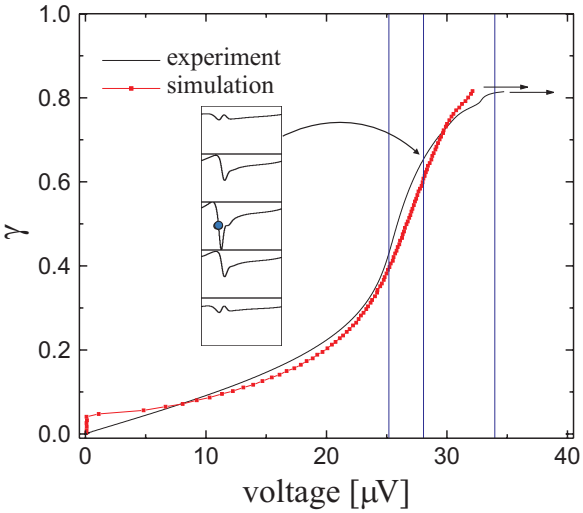

FIG. 11. Measured and simulated CVC of a single fluxon in the center junction of sample #3 at 8K; the inset shows the profile of the phase differences at the marked point, the vertical lines indicate $c_5^{(5)}$, $c_4^{(5)}$ and $c_3^{(5)}$.

C. High damping regime

Increasing the temperature of the sample with the fluxon state shown in Fig. 8 to 8 K increases the quasiparticle conductance to G=174 kS/cm^2. As seen in Fig. 11, Cherenkov radiation is quickly damped and the resonances on the fluxon step vanish. Yet the velocity of the fluxon does not asymptotically reach a certain value as observed for solitons in single junctions. In contrast, an S-shape of the CVC is observed. The absence of a limiting velocity indicates that the fluxon lacks the properties of a relativistic soliton, but it still maintains its topological stability, as indicated in the inset phase distribution.

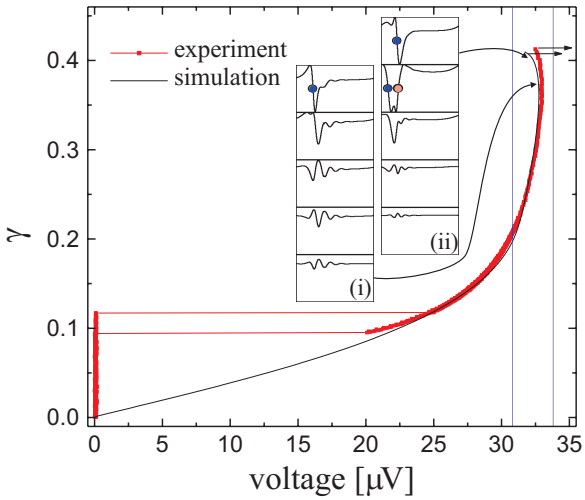

FIG. 12. Measured and simulated CVC of a single fluxon in the strong junction of sample #1: the profiles of the phase differences are shown as insets for the bias points $\gamma_{(i)}$=0.38 and $\gamma_{(iv)}$=0.412, the vertical lines indicate $c_5^{(5)}$ and $c_4^{(5)}$.

The fluxon state shown in Fig. 9 measured at 8 K results in a CVC similar to the one shown in Fig. 11, in particular the negative differential resistance of the fluxon step vanishes. Yet this backbending has been observed recently in twofold stacks by E. Glodobin et al.[8] as well as during this work in sample #1 (see Fig. 12). In both cases it is found that the particular prerequisite to observe backbending is that the fluxon needs to be located in a junction that has a higher critical current than the neighboring one, we call it the strong junction. This condition is sufficient, but not the only necessary one to observe a negative differential resistance in the CVC.

For simulation, the critical current density J was calculated according to the temperature in experiment of 6.8 K to J_5=145 A/cm^2 and $J_{1,\ldots,4}$=90 A/cm^2. The quasiparticle conductances are chosen inhomogeneously, as well. The values of G_5=170 kS/cm^2 and $G_{1,\ldots,4}$=120 kS/cm^2 reflect that both critical current and quasiparticle conductance depend on the barrier quality. Yet we find that backbending occurs in a wide range of conductances: The effect is present, even if G is the same for all layers.

As seen in the insets of Fig. 12, the fluxon is placed in the strong top (l=5) junction and a damped Cherenkov tail originates from it. The image of the fluxon and radiation is seen in the neighboring junctions. At the onset of the of the backbending shown in inset (i), the phase difference in junction l=4 is just above $\pi/2$ (note that the plot shows $\sin\phi_l$ on the ordinate). As the bias current increases, so does the amplitude of the oscillation of the phase differences in this junction. When the amplitude exceeds 2π at $\gamma_{(iv)}$=0.412, a fluxon-antifluxon pair is created. The Lorenz force from the bias current pulls the created vortex and antivortex in opposite directions. An instant later the pair causes the nucleation of further fluxons and antifluxons in all other junctions and an avalanche of particles switches the junction to the

whirling state.

Since the amplitude of the plasma oscillations at the point of the backbending is quite large, the approximation of the small amplitude wave dispersion relation (2.2) is not valid here. As often seen in non-linear systems, the dispersion of a traveling wave then depends on its amplitude. In fact, it has been shown[14] that for single long junctions a large amplidude phase difference leads to an effective reduction of the plasma frequency ω_p. This reduction in plasma frequency effectively decreases the phase velocity $v_{\rm phase}$ of the waves and, therefore, also the fluxon velocity $v_{\rm fluxon}$ locked to the resonance. In the weak coupling limit this model is applicable to stacks, if the amplitude of the radiation in the weak junction gets high. On the other hand, the influence of coupling on the wave dispersion relation is rather hard to address analytically.

IV. CONCLUSION

We have studied the dynamics of single fluxons in 5- and 10-fold stacks of Josephson junctions experimentally, numerically and analytically. The resonances observed at low damping are well explained from the inductive coupling model as Cherenkov radiation. This mechanism governs the motion of the fluxon in the super-relativistic regime: The fluxon velocity locks to the phase velocity of the Cherenkov waves. Increased damping attenuates these waves and broaden their linewidth so that locking of the fluxon velocity is no longer possible. Nonetheless the experimental evidence for the lack of the Lorenz invariance of the coupled sine-Gordon equations (2.1) is observed in the form of an S-shaped CVC. Furthermore we the so-called backbending observed in the CVCs is attributed to the nonlinear effects in the stack.

V. ACKNOWLEDGEMENTS

We'd like to acknowledge N. Thyssen for the fabrication of the 5-fold stacks. The authors are also grateful to E. Goldobin and B.A. Malomed for useful discussions. This work was supported by Deutsche Forschungsgemeinschaft (DFG).

[1] R. Kleiner, F. Steinmeyer, G. Kunkel, and P. Müller, Phys. Rev. Lett. **68**, 2394 (1992).
[2] R. Kleiner, T. Gaber, and G. Hechtfischer, to be submitted to Phys. Rev. B (unpublished).
[3] M. Machida, T. Kozama, A. Tanaka, and M. Tachiki, J. Appl. Phys.? (1999).
[4] S. Sakai *et al.*, Phys. Rev. B **50**, 12905 (1994).
[5] E. Goldobin, A. Wallraff, N. Thyssen, and A. Ustinov, Phys. Rev. B **57**, 130 (1998).
[6] A. Wallraff, E. Goldobin, and A. Ustinov, J. Appl. Phys. **80**, 6523 (1996).
[7] E. Goldobin, B. Malomed, and A. Ustinov, Phys. Lett. A **266**, (2000).
[8] E. Goldobin, A. Wallraff, and A. Ustinov, J. Low Temp. Phys. **119**, 589 (2000).
[9] E. Goldobin, B. Malomed, and A. Ustinov, Phys. Rev. B (2000), in press.
[10] S. Sakai, P. Bodin, and N. Pedersen, J. Appl. Phys. **73**, 2411 (1993).
[11] S. Sakai, A. Ustiov, N. Thyssen, and H. Kohlstedt, Phys. Rev. B **58**, 5777 (1998).
[12] J. Zitzmann, Master's thesis, Universität Erlangen-Nürnberg, 2000, http://www.physik.uni-erlangen.de/pi3/ustinov/publications.
[13] S. Keil *et al.*, Phys. Rev. B **54**, 14948 (1996).
[14] A. Ustinov, B. Malomed, and E. Goldobin, Phys. Rev. B **60**, 1365 (1999).

TABLES

TABLE I. Junction properties of the measured samples

sample	layers N	length [μm]	thicknesses of the Nb films [nm]			critical current density
			top	intermediate	bottom	at 4.2 K [A/cm^2][a]
1	5	416	180	90	90	90
2	5	416	180	90	90	130
3	5	416	180	90	90	140
4	5	597	180	90	90	140
5	10	416	120	60	90	81
6	10	597	120	60	90	81

[a]The spread of the critical current density in all samples is below 5%, except for sample #1, where one of the junctions has a critical current density of 145A/cm^2.

This publication is based (partly) on the presentations made at the European Research Conference (EURESCO) on "Future Perspectives of Superconducting Josephson Devices: Euroconference on Physics and Application of Multi-Junction Superconducting Josephson Devices, Acquafredda di Maratea, Italy, 1-6 July 2000, organised by the European Science Foundation and supported by the European Commission, Research DG, Human Potential Programme, High-Level Scientific Conferences, Contract HPCFCT-1999-00135. This information is the sole responsibility of the author(s) and does not reflect the ESF or Community's opinion. The ESF and the Community are not responsible for any use that might be made of data appearing in this publication."